

# Open and coastal seas interactions south of Japan represented by an ensemble Kalman filter

Yasumasa Miyazawa · Toru Miyama ·  
Sergey M. Varlamov · Xinyu Guo · Takuji Waseda

Received: 4 August 2011 / Accepted: 21 December 2011 / Published online: 2 February 2012  
© Springer-Verlag 2012

**Abstract** We investigated the feasibility of the ensemble Kalman filter (EnKF) to reproduce oceanic conditions south of Japan. We have adopted the local ensemble transformation Kalman filter algorithm based on 20 members' ensemble simulations of the parallelized Princeton Ocean Model (the Stony Brook Parallel Ocean Model) with horizontal resolution of  $1/36^\circ$ . By assimilating satellite sea surface height anomaly, satellite sea surface temperature, and in situ temperature and salinity profiles, we reproduced the Kuroshio variation south of Japan for the period from 8 to 28 February 2010. EnKF successfully reproduced the Kuroshio path positions and the water mass property of the Kuroshio waters as observed. It also detected the variation of the steep thermohaline front in the Kii Channel due to the intrusion of the Kuroshio water based on the observation, suggesting efficiency of EnKF for detection of open and coastal seas interactions with highly complicated spatiotemporal variability.

**Keywords** Ensemble Kalman filter · Kuroshio · Kii channel front · OGCM

## 1 Introduction

Variability of geophysical systems is highly chaotic (Lorenz 1963). An ultimate goal of geophysical predictability studies is to exactly evaluate probability distributions associated with target phenomena. The ensemble Kalman filter (EnKF; Evensen 1994) is based on the Monte Carlo method using ensemble model simulations. It allows dynamical update of two important moments of the probability distribution: mean and error covariance. Applications of EnKF have covered a wide range of research fields because of its simple implementation and effectiveness (Evensen 2003).

So far, there have been no studies on EnKF for the analysis of the Kuroshio variations south of Japan. Other types of data assimilation methods frequently used for operational applications to the Kuroshio variations: optimum interpolation (Miyazawa et al. 2005; 2008) and three-dimensional variational method (Miyazawa et al. 2009) assumed temporally constant and spatially isotropic error covariance. Main target phenomena of the previous studies were the typical mesoscale phenomena such as the Kuroshio path variation and mesoscale eddies with O (10 days) and O (100 km) scales. Recent development of downscaled models allows simulating smaller scales phenomena associated with the Kuroshio and coastal topography interactions (Miyama and Miyazawa 2010). The open and coastal seas interactions involve significant variations of temporal and spatial scales of the relevant phenomena (e.g., Isobe et al. 2010), and the associated error covariance is also highly variable. Dynamic representation of error covariance by EnKF is hence required to effectively reproduce the open and coastal seas

---

Responsible Editor: Leo Oey

---

This article is part of the Topical Collection on the *3rd International Workshop on Modelling the Ocean 2011*

---

Y. Miyazawa (✉) · T. Miyama · S. M. Varlamov · X. Guo ·  
T. Waseda

Research Institute for Global Change, Japan Agency for Marine-  
Earth Science and Technology, Yokohama,  
3173-25 Showamachi, Kanazawa-ku,  
Yokohama, Kanagawa 236-0001, Japan  
e-mail: miyazawa@jamstec.go.jp

X. Guo  
Center for Marine Environmental Studies, Ehime University,  
Matsuyama, Ehime 790-8577, Japan

T. Waseda  
Graduate School of Frontier Science, The University of Tokyo,  
Kashiwa, Chiba 277-8563, Japan

interactions. This study aimed to elucidate the feasibility of EnKF for the analysis of the Kuroshio variations south of Japan, especially focusing on roles of error covariance information in representation of the Kuroshio and coastal sea interactions.

The temporal and spatial sampling intervals of the remote sensing observations are approximately regular, and their sampling coverage is mainly limited in open oceans. This is one of main reasons that the operational ocean forecasting for open oceans has been established over the past decade (Miyazawa et al. 2009). Full utilization of the in situ temperature and salinity data locally and irregularly sampled near the coast is crucial for establishing the ocean forecast of the open and coastal seas interactions. Our research interests include roles of the dynamic representation of the forecast error covariance in assimilating the localized in situ observation data.

The Kii Channel between the Shikoku Island and Kii Peninsula (Fig. 1) has approximately 50 m bottom depth. In winter, very steep oceanic front, ‘Kii Channel Front’, is formed due to convergence of warm-salty water from open ocean and cold-fresh water from coastal regions (Yosioka 1983). The S-shape front is frequently generated due to the Coriolis effect (Harashima and Oonishi 1981). The existence of these fronts is recognized in many areas of the western North Pacific including Tokyo Bay (Yanagi and Sanuki 1991), Ise Bay (Yanagi et al. 1997), and the South China Sea coasts (Wang et al. 2001). In the Kii Channel, the Kuroshio water intrusions frequently affect the front

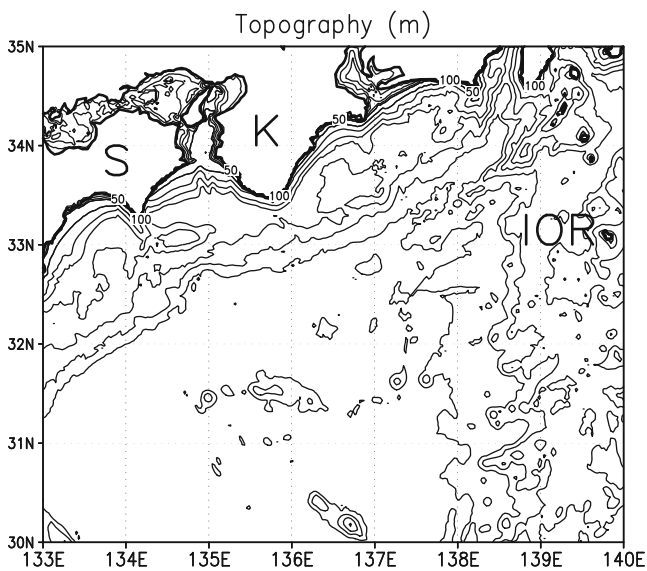


**Fig. 1** Topography of the model domain. *Thick (thin)* contours denote shorelines (iso-depth lines: 10, 20, 30, 40, 50, 100, 200, 500, 1,000, 2,000, 3,000, 4,000, and 5,000 m). The abbreviations represents locations (*S* Shikoku Island, *K* Kii Peninsula, and *IOR* Izu-Ogasawara Ridge). The Kii Channel is between the Shikoku Island and Kii Peninsula

variations and sometimes disturb the stable condition of the S-shape front (Toda 1992). This study examined the reproducibility by EnKF of the Kuroshio and its related Kii Channel Front variations in February 2010.

This paper is organized as follows. Section 2 provides brief descriptions of an ocean model and an implementation of EnKF in the present study. Section 3 discusses the reproducibility of the Kuroshio south of Japan and Kii Channel Front in February 2010. Impact of localized in situ data assimilation and predictability of the front variations are discussed in Sections 4 and 5 in terms of time-dependent anisotropic error covariance represented by EnKF. Section 6 is devoted to summary and discussion.

## 2 Ensemble Kalman filter system

We have developed an ocean model for south of Japan based on a parallelized version of the Princeton Ocean Model (Stony Brook Parallel Ocean Model, sbPOM; available from <http://www.imedea.uib-csic.es/users/toni/sbpom/>). The model covers a square region of 31°–35° N and 133°–140° E (Fig. 1) with a horizontal resolution of 1/36° and 31 sigma levels in vertical. The bottom topography of the model was created from the 1/120° grid data provided by Japan Hydrographic Association, ‘JTOPO30’. The model was driven by wind and heat fluxes calculated using the bulk formulae (Kagimoto et al. 2008) with 6-hourly atmospheric variables provided from the National Centers for Environmental Prediction Global Forecast System (NCEP GFS). The surface salt flux was relaxed to surface salinity of the monthly mean climatology, World Ocean Atlas 2001 (Conkright et al. 2002) with a restoring rate of 10 m/30 days. The lateral boundary condition was specified from the JAMSTEC operational ocean model product with the same horizontal resolution of 1/36° (Miyama and Miyazawa 2010), which assimilated satellite sea surface height anomaly data using a three-dimensional variational method (Miyazawa et al. 2009). Tide forcing was not included in the model. Note that not only the data assimilation module but also the forcings and/or numerical schemes are effective to improve the representation skill for the open and coastal seas interactions. But our focus in the present study is to investigate the roles of the data assimilation in the skill improvements. The model was spun up for the period from November 2008 to March 2010 starting from temperature and salinity data of the JAMSTEC operational model on 1 November 2008 with no motion.

We have implemented the Local Ensemble Transformation Kalman Filter (LETKF; Hunt et al. 2007; Miyoshi et al. 2010) algorithm on the JAMSTEC scalar parallel processors system on the basis of SGI Altix 4700. Twenty numbers of ensemble runs were produced using different initial

conditions sampled from the background simulation data with time interval of 3 days during the simulation period from 13 January to 11 March 2010.

Here we briefly describe the formulation of LETKF (Hunt et al. 2007). The ensemble mean of the analyses is obtained by the following equation,

$$\bar{x}^a = \bar{x}^f + X^f w^a, \tag{1}$$

where  $\bar{x} = \sum_{i=1}^K \frac{x_i}{K}$ , size of the ensemble is  $K$ ,  $x^f(x^a)$  is a  $m$ -dimensional vector representing each member of ensemble forecasts (analyses),  $X^f$  is a  $m \times K$  matrix that is composed of  $K$ -number columns of deviations of the forecasts from the ensemble mean of the forecasts, and  $w^a$  is a  $K$ -dimensional vector calculated from the observation data and ensemble forecasts. Update of each analysis member is represented as follows,

$$x^{a(i)} = \bar{x}^a + X^f W^{a(i)}, \tag{2}$$

where  $W^{a(i)}$  is a  $K$ -dimensional vector corresponding to  $i$ th column of a  $K \times K$  matrix  $W^a$ , calculated from the ensemble forecasts. Not only the ensemble mean but also the ensemble spread,

$$\text{Sprd} = \sqrt{\sum_{i=1}^K \frac{(x_i - \bar{x})^2}{K}}, \tag{3}$$

provides the useful information for the predictability analysis.

Localized use of observation data is one of key methodologies of LETKF (Hunt et al. 2007). We defined two localization scales (Miyoshi et al. 2010):

$$\text{dist}_{\text{zero}} = \sigma_{\text{obs}} \cdot \sqrt{10/3} \cdot 2, \quad \text{dist}_{\text{zerov}} = \sigma_{\text{obsv}} \cdot \sqrt{10/3} \cdot 2, \tag{4}$$

where  $\sigma_{\text{obs}}$  (grid number) and  $\sigma_{\text{obsv}}$  (m) are horizontal and vertical localization scales, respectively. Observation data far from the target grid with horizontal distance (dist) larger than  $\text{dist}_{\text{obs}}$  or vertical distance (distv) larger than  $\text{dist}_{\text{obsv}}$  were not used for the EnKF analysis there. In addition, observation errors of the data far from the target grid were enhanced by multiplying a factor,  $\exp(0.5 \cdot ((\text{dist}/\text{dist}_{\text{obs}})^2 + (\text{distv}/\text{dist}_{\text{obsv}})^2))$ .

LETKF assimilated satellite sea surface height anomaly (Jasons-1 and Jasons-2), satellite sea surface temperature (NOAA MCSST and AMSR-E), and in situ temperature and salinity profiles (GTSP) every 2 days during the target period from 8 to 28 February 2010. All sea surface height anomaly (temperature and salinity) data obtained during the period from 4 days (1 day) before the analysis time to the

same days after were used for one time filter analysis (seventh and eighth rows of Table 1). Figure 2 plots the observation data points used in the LETKF analyses on 14 (Fig. 2a), 20 (Fig. 2b), and 26 (Fig. 2c) February 2010. Data points of the remote sensing observations (sea surface height anomaly and sea surface temperature) were regularly distributed in open ocean. Numbers of in situ observation data were generally few but sometimes the data points were locally and densely distributed around the Kii Channel (see Fig. 8). Mean sea surface height for evaluation of model sea surface height anomaly, which is an important parameter of the satellite altimetry data assimilation (Miyazawa et al 2009), was calculated from the hindcast data of the JAMSTEC operational model for the period from 1 August 2009 to 1 August 2010.

Parameters of LETKF (Miyoshi et al. 2010) were determined (Table 1) based on examination of their sensitivity using ‘identical twin experiments’, in which pseudo-observation data were sampled from the background simulation data, and quantitative skill evaluation for each parameter using known ‘true’ state was feasible. The observation errors shown in Table 1 are not simple measurement errors but include the representativeness errors associated with unresolved smaller scales variability and model discretization (Cohn 1997). Since the LETKF analysis was conducted every 2 days, which was not so long a time to induce the typical bimodality of the Kuroshio path variations (Miyazawa et al. 2005), it was not necessary to consider the possibility of non-Gaussian type probability distributions that were not simply described by mean and error covariance mainly targeted by the Kalman filter analysis.

To examine the data assimilation effects of EnKF and its implications on representation of open and coastal seas interactions, we have conducted following experiments: (1) the basic case, ‘ENKF’, (2) the free running forecasts

**Table 1** LETKF parameters

Horizontal localization scale ( $\sigma_{\text{obs}}$ ; number of grids)	12 (1/3 degree)
Vertical localization scale ( $\sigma_{\text{obsv}}$ ; m)	2,000
Covariance inflation parameter (%)	21
Observation error of sea surface height anomaly (m)	0.2
Observation error of temperature (°C)	1.0
Observation error of salinity (psu)	0.1
Time window of sea surface height anomaly (day)	±4
Time window of temperature and salinity (day)	±1
Time interval of LETKF (day)	2

Positive covariance inflation parameter means that the forecast ensemble spread is inflated by a factor slightly greater than unity (Miyoshi et al. 2010). Miyazawa et al.: Open and coastal seas interactions represented by EnKF

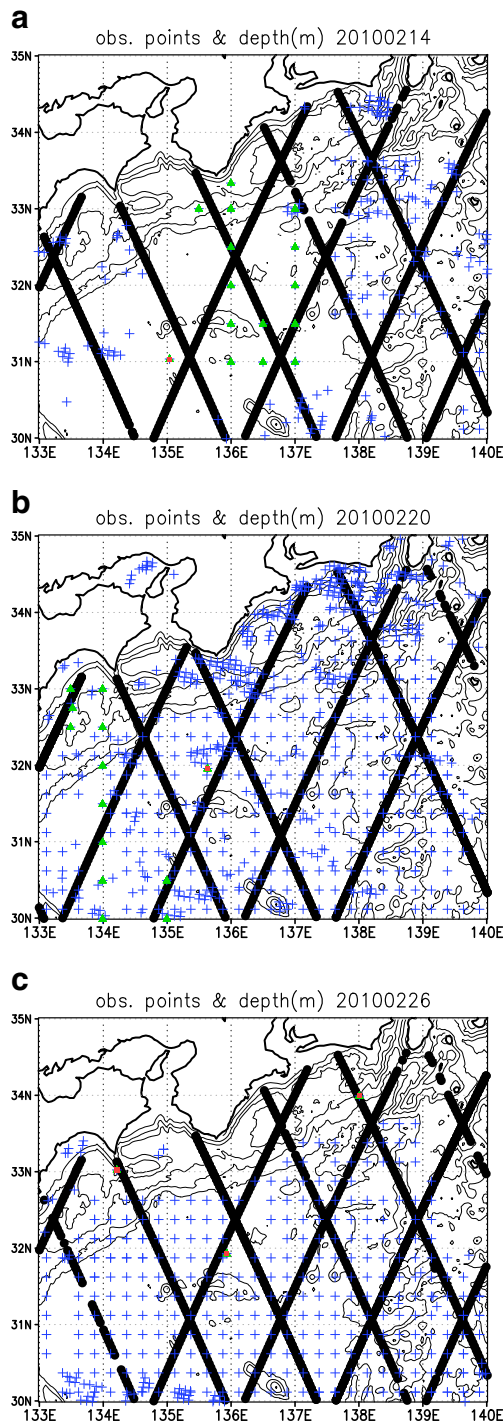


**Fig. 2** Positions of the observation data assimilated on **a** 14 February 2010, **b** 20 February 2010, and **c** 26 February 2010. Closed circles satellite sea surface height anomaly. Crosses satellite sea surface temperature. Closed triangles in situ temperature. Closed squares in situ salinity. Thick contours in background denote iso-depth lines of 200, 500, 1,000, 2,000, 3,000, 4,000, 5,000, and 6,000 m

produced by running the ensemble runs without any data assimilation, ‘FRF’, and (3) EnKF without in situ data assimilation ‘NO IN SITU’.

### 3 Reproduced oceanic condition south of Japan in February 2010

In this section, we discuss the general skill of EnKF by comparing the Kuroshio path variations and water mass variability with their observations. Synthetic sea surface temperature maps provided by Japanese local fishery agencies around the Kuroshio region (Xie et al. 2006) indicate that the small Kuroshio meander around 33° N and 138° E observed on 14 February 2010 (Fig. 3a) moved eastward to around 140° E on 26 February (Fig. 3c). The Kii Channel Front was formed between the colder and warmer waters in northern and southern sides, respectively (Figs. 3a–c). The warmer water in the southern side of the front intruded northward into the channel on 14 and 26 February (Fig. 3a, c), but on 20 February, the warmer waters moved southward out of the channel.

The ENKF analysis mean (see Eq. 1) reasonably reproduced these features as shown in Fig. 4. The small meander of the Kuroshio moved eastward during the period, and the variation of the Kii Channel Front was generally reproduced. ENKF basically represented the typical S-shape front characterized by the colder (warmer) temperature in western (eastern) side of the channel throughout the target period. However, the observation maps indicate that the opposite shape of the front with the colder (warmer) temperature in eastern (western) side of the channel occurred for the periods from 8 to 10 (not shown) and from 20 to 23 February (e.g., see Fig. 3b). We note that the synthetic observation maps (Fig. 3) were not completely independent from ENKF, because they included the remote sensing sea surface temperature data as same as those used for the EnKF analysis. But production of them involved many other data including in situ observations and manual modifications based on empirical knowledge about oceanic conditions south of Japan (Xie et al. 2006).

We compared the reproduced Kuroshio path portions of ENKF with the positions evaluated by the Japan Coast Guard (JCG Kuroshio axis positions) defined as the strongest flow positions in the Kuroshio flow band. The modeled path positions denoted by the thick lines shown in Fig. 5 were defined as the grid positions of strongest kinetic energy at 50 m depth. Root mean square deviation (RMSD) between ENKF and JCG Kuroshio axis positions was 0.27° for the target period. The JCG Kuroshio path positions also show the propagation of the small meander depicted in both the ENKF analyses and synthetic maps (Fig. 3). ENKF reproduced the smaller amplitude of the meander as compared to that indicated by the JCG Kuroshio path positions.

To confirm fitting to the in situ data of the assimilation products, we plotted in upper (lower) panels of Fig. 6 the in situ observation points with colors indicating RMSD between the reproduced and observed vertical temperature

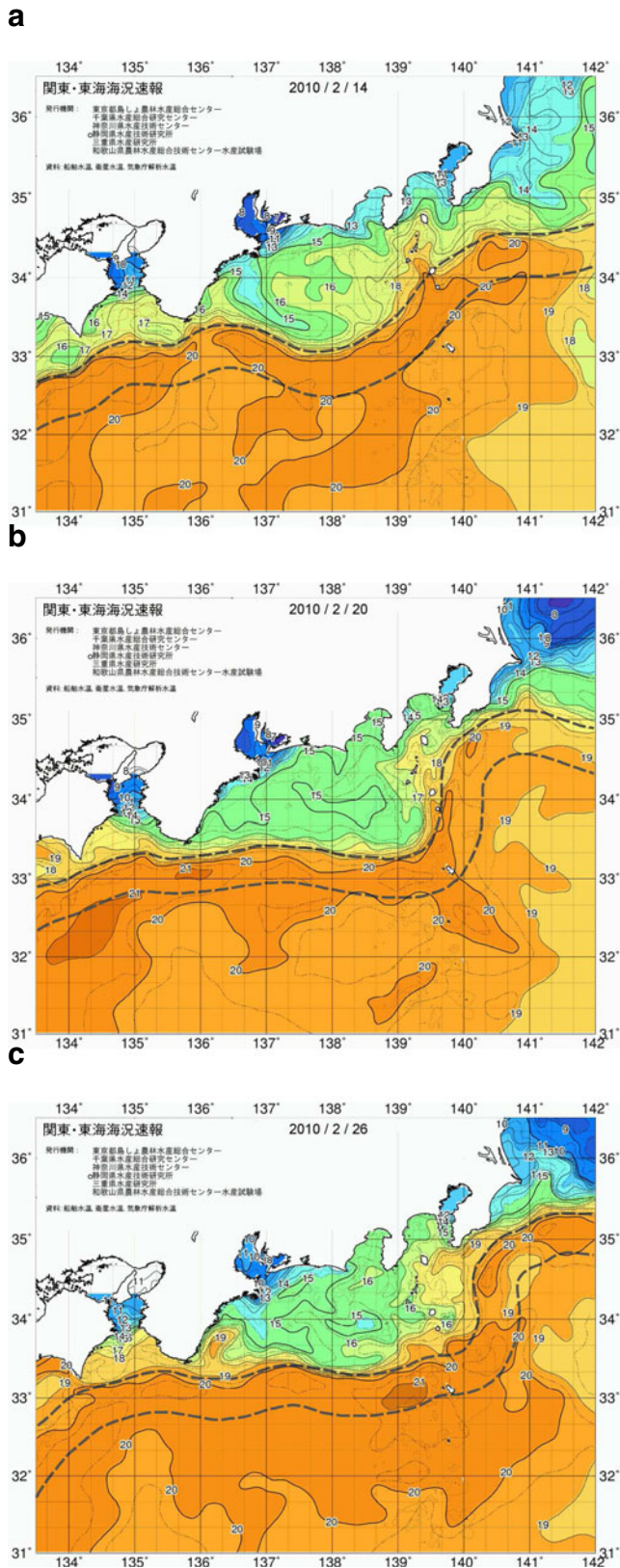


**Fig. 3** Synthetic maps of sea surface temperature observations (Xie et al. 2006) on **a** 14 February 2010, **b** 20 February 2010, and **c** 26 February 2010, provided by local fishery research agencies around the mapping area. *Thick dashed lines* denote northern and southern edges of the Kuroshio

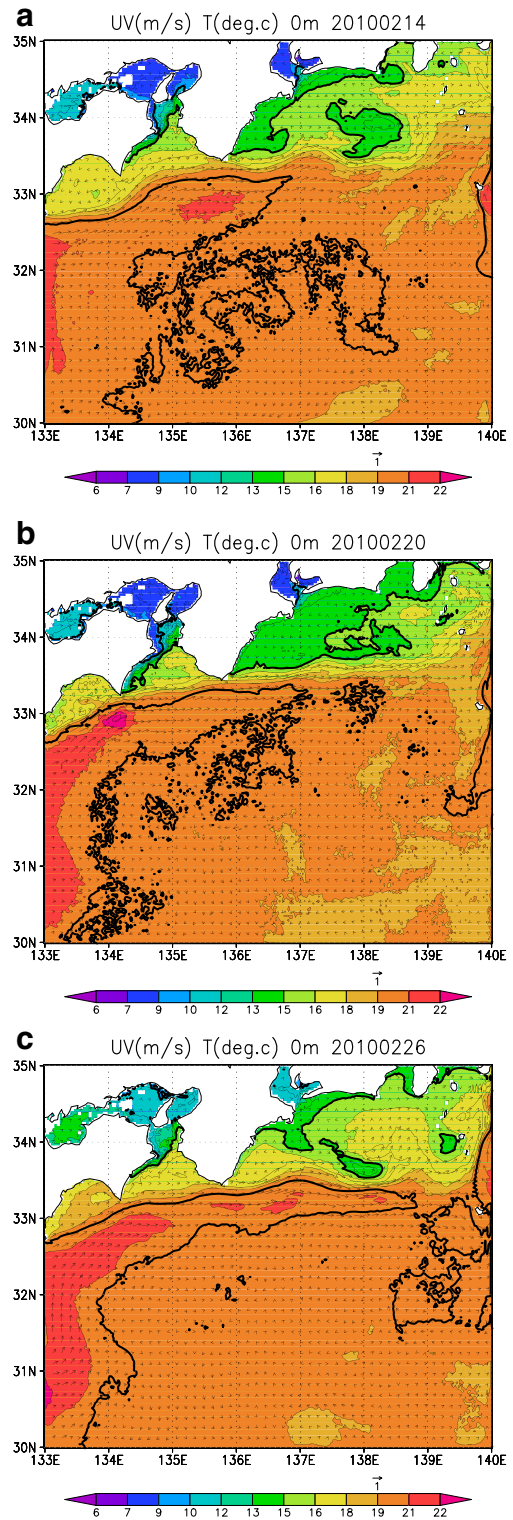


**Fig. 4** Ensemble mean sea surface temperature (*shade and contours*) and flows (*vectors*) of the ENKF analyses on **a** 14 February 2010, **b** 20 February 2010, and **c** 26 February 2010

(salinity) profiles. ENKF (Fig. 6a) well reproduced the observed water mass in open ocean with RMSD smaller than 1°C and 0.1 psu, which are the prescribed observation

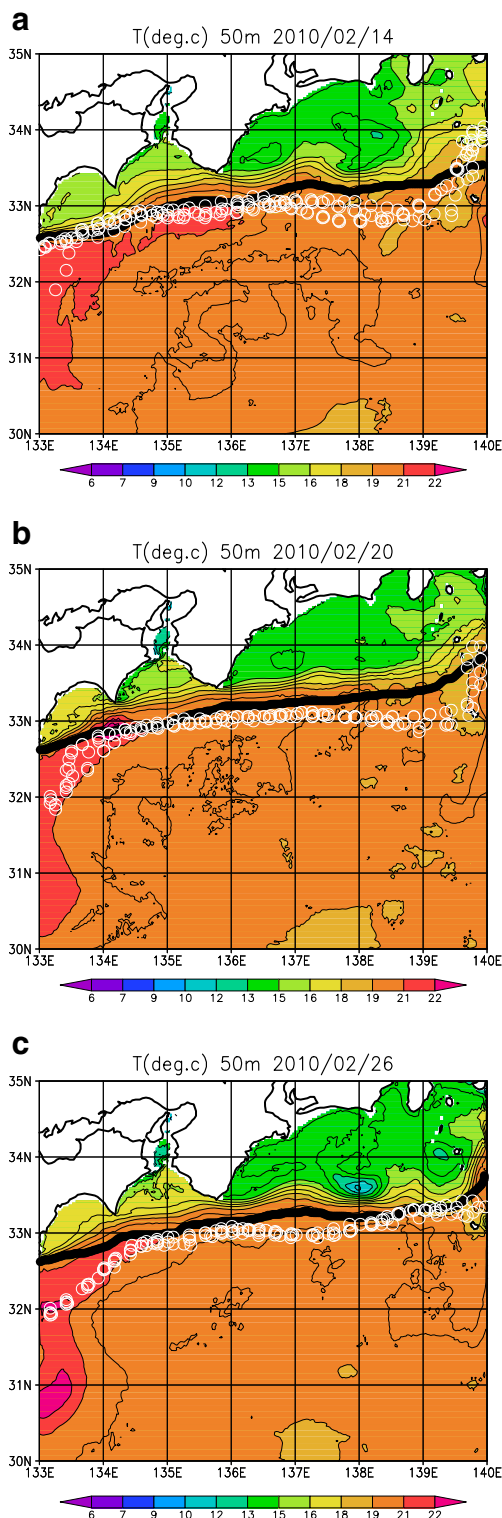


**Fig. 5** Same as Fig. 4 except for temperature at 50 m depth. *Thick contours* denote the Kuroshio path positions evaluated from the ensemble mean flows at 50 m depth by tracking grids with the strongest kinetic energy at each longitude. *Open circles* represent the weekly mean observed path positions provided from the Japan Coast Guard. The duration of the weekly mean period was daily updated and then all position data including the target day in their weekly mean periods were plotted

error values (Table 1). Comparatively large RMSD values indicated by red color contours are shown near the coast, especially inside of the Kii Channel. Ensemble spread (3) of maximum temperature in the vertical column plotted in background of upper panels of Fig. 6a exhibits that large magnitude of the spread is distributed along the Kuroshio path and coastal seas including the Kii Channel. Large values of salinity spread (lower panels of Fig. 6a) are shown in the coastal seas. Comparatively large values of RMSD and bias are found around the Kii Channel, and the magnitude of the spread there is also large. This kind of errors is possible because the real horizontal gradient of the Kii Channel Front is very steep, usually exceeding  $5^{\circ}\text{C}/\text{km}$  (Yosioka 1983), and it is difficult to exactly represent it by hydrostatic dynamics of the present model framework with the horizontal resolution of  $1/36^{\circ}$ , approximately 3 km (Akitomo et al. 1990).

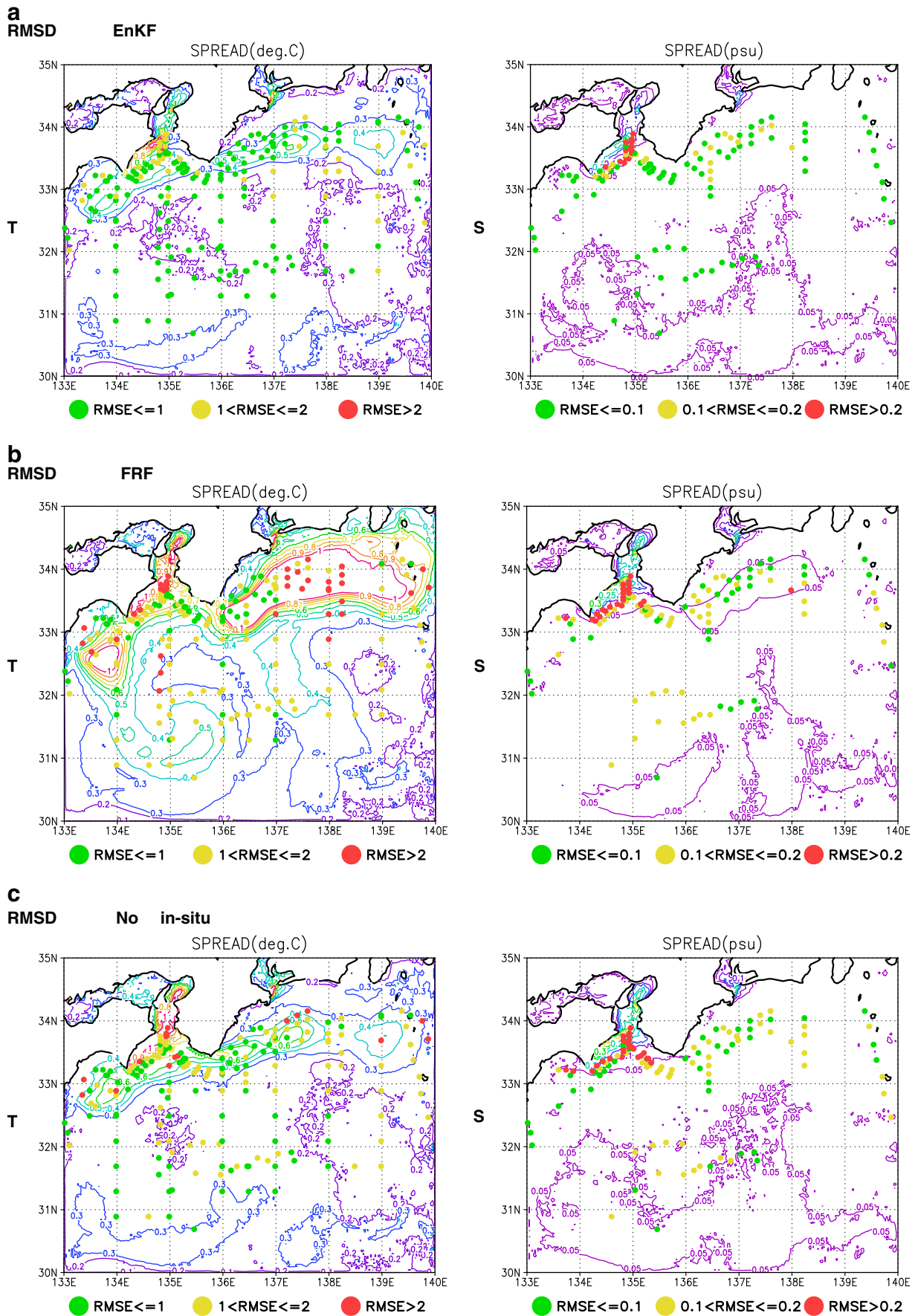
Comparison between the skills of ENKF (Fig. 6a) and FRF (Fig. 6b) indicates that the data assimilation effectively reduced RMSD and the magnitude of ensemble spreads, suggesting some relations between skills and ensemble spreads. In particular, the data assimilation corrected warm bias near the coast (Fig. 7) by suppressing the tendency of the Kuroshio water intrusion toward the coast represented in FRF. Note that RMSD between the Kuroshio path positions of the ensemble mean of FRF and JCG was  $0.39^{\circ}$ , larger than RMSD ( $0.27^{\circ}$ ) between EnKF and JCG. The mean Kuroshio path of FRF during the target period showed unrealistic troughs and ridges south of Japan (Fig. 7).

The case without in situ data assimilation (NO IN SITU; Fig. 6c) exhibits improvements of water mass property and reduction of the ensemble spread as compared to FRF (Fig. 6b). Figure 6c demonstrates the skill improvement by comparing the results with the ‘independent’ data because the in situ data was not assimilated into the NO IN SITU case. Inside of the Kii Channel, the water mass property was not improved and magnitude of the spread was unchanged due to low density of the remote sensing data there (Fig. 2). RMSD between the Kuroshio path positions of the ensemble mean of NO IN SITU and JCG was  $0.28^{\circ}$ , slightly larger than that of ENKF ( $0.27^{\circ}$ ).

#### 4 Assimilation of the in situ observation data by EnKF

Temporal frequency and spatial density of the in situ temperature and salinity observation were irregular as compared to those of the remote sensing data (e.g., Fig. 2). Sometimes in

**Fig. 6** Maximum analysis ensemble spread from surface to bottom averaged for the period from 8 to 28 February 2010. *Left* temperature, *right* salinity. *Closed circles* denote all positions of the in situ observations whose numbers were larger than 4 and their *colors* indicate root mean square deviation between the reproduced and observed in situ profiles. **a** ENKF, **b** NO IN SITU, **c** FRF



situ data were distributed locally and densely. Figure 8 shows that the in situ temperature and salinity were observed densely inside of the Kii Channel around 18 February 2010. In particular, since the altimetry data were basically unavailable in the coastal regions due to their low quality (Vignudelli et al.

2000), the in situ data around the coastal regions were quite important for the reproduction of the oceanic condition there. Using information of the ensemble means, we can evaluate impacts of the in situ data assimilation. Impact signal (IS) of the assimilation is defined as

$$IS \equiv \begin{cases} \bar{x}_w - \bar{x}_{w/o} & \text{if } |\bar{x}_w - \bar{x}_{w/o}| / \sqrt{(\text{Spread}_w^2 + \text{Spread}_{w/o}^2)/(K-1)} > t_{95\%} \\ 0 & \text{not} \end{cases} \quad (5)$$

where  $\bar{x}_w - \bar{x}_{w/o}$  is difference of ensemble mean variables between with ( $w$ ) and without ( $w/o$ ) the assimilation of some observation data,  $K$  is ensemble size ( $=20$ ), and  $t_{95\%}$  is a

critical  $t$ -distribution value of 95% significance with  $K-1$  degree of freedom (Moteki et al. 2011). IS of sea surface temperature and salinity between with (ENKF) and without (NO IN SITU) the assimilation of the in situ temperature and salinity profiles on 18 February were plotted in Figs. 9a and b, respectively. ISs of temperature and salinity were almost similar to each other. Positive (negative) anomaly is found along the west coast of the Kii Peninsula (inside of the Kii Channel), indicating that the in situ data assimilation enhanced the intensity of the Kii Channel Front. In particular, positive anomaly along the west coast of the Kii Peninsula contributed to reproduce the anti-clockwise circulation of the Kuroshio water intrusion (Figs. 9c and d). Warm water patches corresponding to the warm water intrusion was also identified in the synthetic observation maps provided by Japanese local fishery agencies for the period from 18 to 19 February 2010 (not shown). Positive IS of temperature and salinity around  $33.3^\circ \text{N}$ ,  $135.4^\circ \text{E}$  at the main axis of the Kuroshio came from the upstream in situ observation of temperature at  $33^\circ \text{N}$ ,  $135^\circ \text{E}$  shown in Fig. 8. The temperature observation affected IS of salinity around there through a multivariate assimilation effect of EnKF, which allowed evaluating a variable by the observations of different kinds of variables.

### T-BIAS

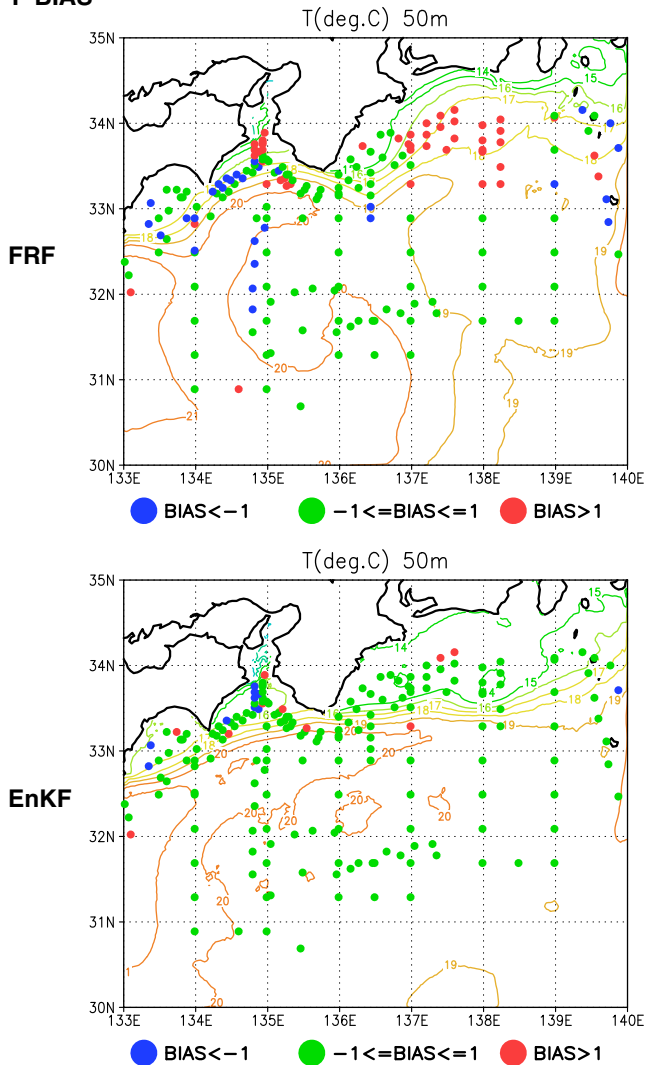


**Fig. 7** Temperature at 50 m depth averaged for the period from 8 to 28 February 2011. Closed circles denote all positions of the in situ observations whose numbers were larger than 4 and their colors indicate mean error (bias) between the reproduced and observed in situ profiles. Upper FRF, lower ENKF

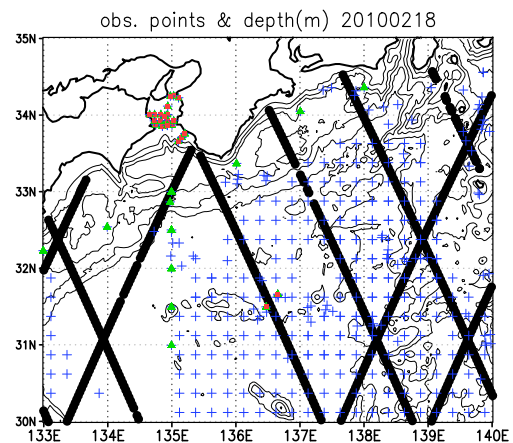


**Fig. 8** Same as Fig. 2 except for 18 February 2010

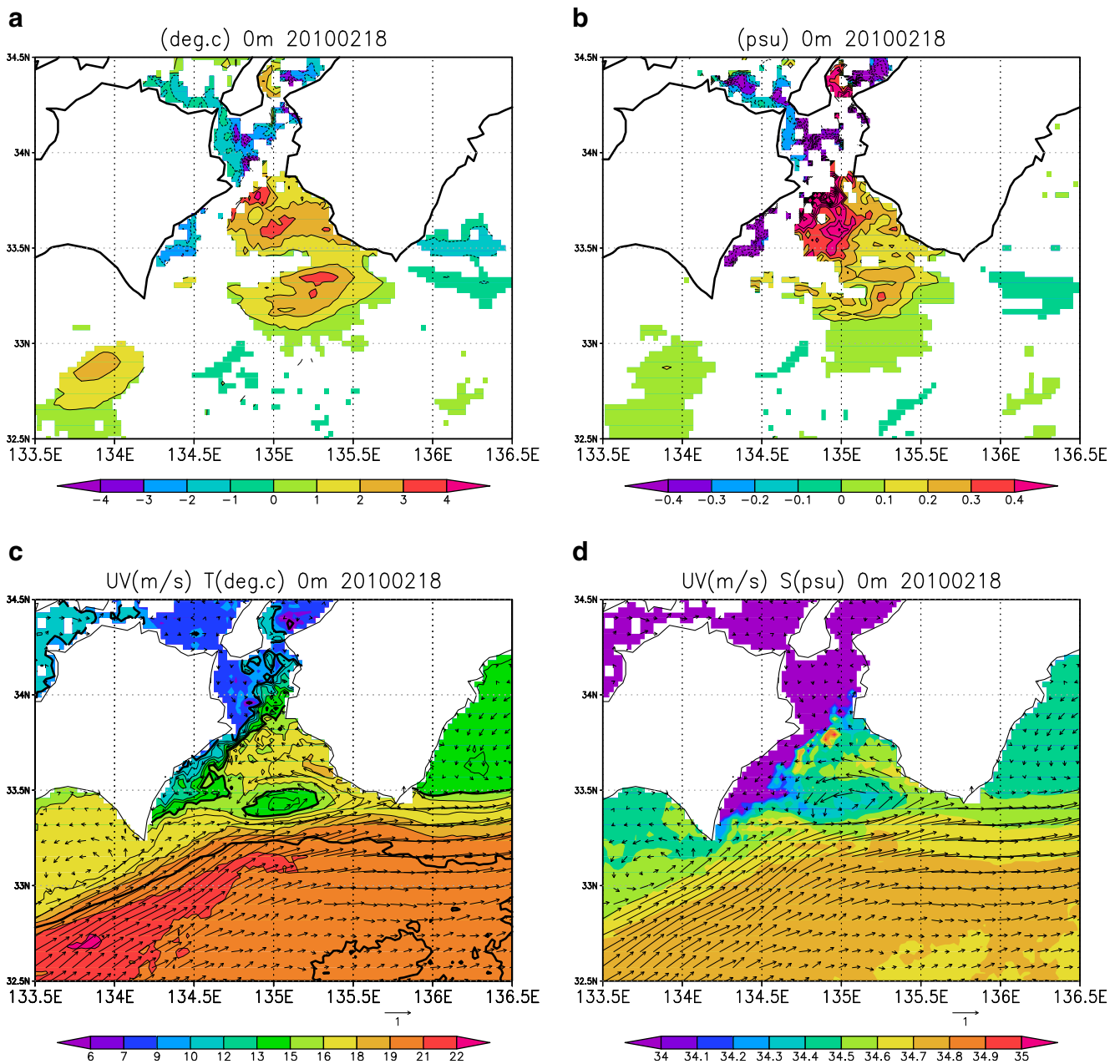


**Fig. 9** **a** Impact signal (5) of ensemble mean of sea surface temperature analyses on 18 February 2010 with (ENKF) and without (NO IN SITU) in situ temperature and salinity profiles. **b** Same as Fig. 9a

except for salinity. **c** Ensemble mean of sea surface temperature analyses in ENKF on 18 February 2010. **d** Same as Fig. 9c except for salinity

To examine possible relations between the horizontal distribution of IS and the forecast error covariance represented by EnKF, we plotted some components of forecast error covariance in Fig. 10,

$$P^f(V_1(x_0), V_2(x)) \equiv (K - 1)^{-1} \sum_{i=1}^K (V_1(x_0)^{(i)} - \overline{V_1(x_0)})(V_2(x)^{(i)} - \overline{V_2(x)}), \tag{6}$$

where  $V_1(x_0)$  ( $V_2(x)$ ) is a value of variable  $V_1$ ( $V_2$ ) at a grid  $x_0$  ( $x$ ), and overbar denotes ensemble mean. We can consider

that upper (lower) panel of Fig. 10 visualizes covariance between an observation of surface temperature (salinity) at a point ( $33.705^\circ$  N,  $135.162^\circ$  E) indicated by a closed circle and surface temperature (salinity) at grids that surround the observation point. The horizontal covariance distributions of temperature and salinity were almost similar to each other as the comparison of IS (c.f. Figs. 9a, b). A positive region shown in the warmer (offshore) side of the Kii Channel Front was associated with the Kuroshio water intrusion along the west coast of the Kii Peninsula (Figs. 9c, d).

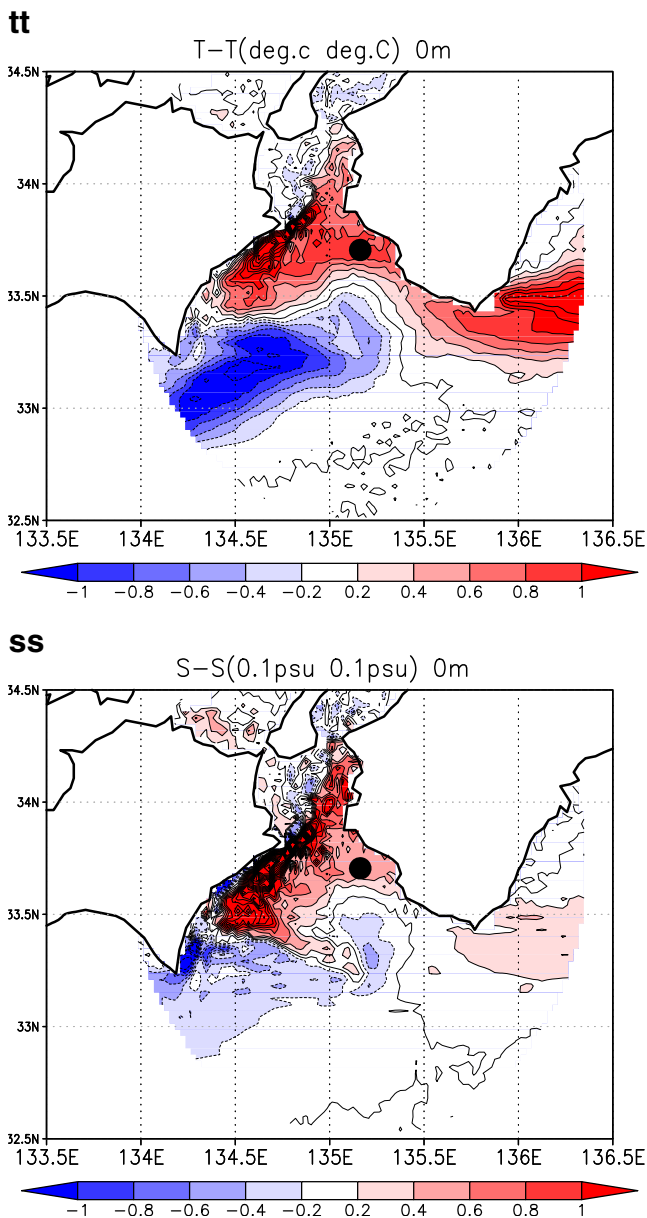


**Fig. 10** Upper the forecast error covariance of ENKF between sea surface temperature at a target point (33.705° N, 135.162° E) and sea surface temperature at surrounding grids on 18 February 2010. Lower same as upper left panel except for sea surface salinity. Values on the grids with distance from the target point larger than  $\text{dist}_{\text{zero}}$  (4) are not shown

Positive covariance region appeared in only the warmer side of the front, suggesting that the observation at the point hardly affected the oceanic state in the colder side of the front. The salinity covariance showed a slightly different feature around 33.3° N, 134.8° E (lower panel of Fig. 10) as compared to the temperature covariance (upper panel of Fig. 10), which was related with a small scale front variation of salinity around there. Negative covariance around 33.2° N, 134.5° E did not affect IS there, suggesting that the impacts from the in situ observations at the other places and/or the

spatial localization scales (4). The distribution of the covariance between temperature (salinity) at the target point and salinity (temperature) at the surrounding grids (not shown) was similar to that of the salinity (temperature) covariance shown in upper (lower) panel, suggesting the effectiveness of the multivariate assimilation effect of EnKF.

Figure 10 indicates that the horizontal distributions of the covariance were strongly related to the basic structures of the oceanic conditions (Figs. 9c, d). In particular, the positive region around the target point was associated with the Kuroshio water intrusion along the west coast of the Kii Peninsula. The positive region almost disappeared on the other analysis days after and before 18 February since the Kuroshio water intrusion did not occur at those times (not shown).

To examine comprehensive impacts of the in situ data assimilation during the whole period, we evaluated reduction rate of the analysis ensemble spread (Moteki et al. 2011) defined as

$$100 \times \frac{\text{Sprd}_{w/o}^2 - \text{Sprd}_w^2}{\text{Sprd}_{w/o}^2} \times \frac{N_s}{N} \quad [\%], \quad (7)$$

where  $\text{Sprd}_{w(w/o)}$  denotes the analysis ensemble spread with (without) the in situ data assimilation.  $N$  is number of all grids, and  $N_s$  is number of grids where the reduction of spread is diagnosed to be significant at 95% level of confidence by  $F$  test. The reduction of ensemble spread could be a qualitative indication of actual error reduction. The reduction rates of temperature averaged for the target period shown in Fig. 11 indicate the reduction of the spread over the whole model region. The reduction was clearly found inside of the Kii Channel. Patterns of the reduction of temperature (Fig. 11) and salinity (not shown) spreads were almost similar to each other but the magnitude of salinity spread reduction was generally larger than that of temperature.

## 5 Ensemble forecasts of the Kii channel front variation

We further investigated impacts of the in situ observation on detecting the Kii Channel Front variation by analyzing the ensemble forecasts around the Kii Channel front region. Figure 12 compares snapshots on 20 February 2010 of a composite map of satellite sea surface temperature provided by the fishery research institute of Tokushima Prefecture (Fig. 12a), an ensemble mean of sea surface temperature and flows of forecasts after 2 days starting from the ENKF analyses at 0:00, 18 February 2010 (Fig. 12b), and that of FRF (Fig. 12c). The ensemble mean forecast of ENKF (Fig. 12b) reproduced the anti-cyclonic circulation due to the Kuroshio water intrusion along the west and east coasts of the Kii Peninsula and Shikoku Island, respectively, as

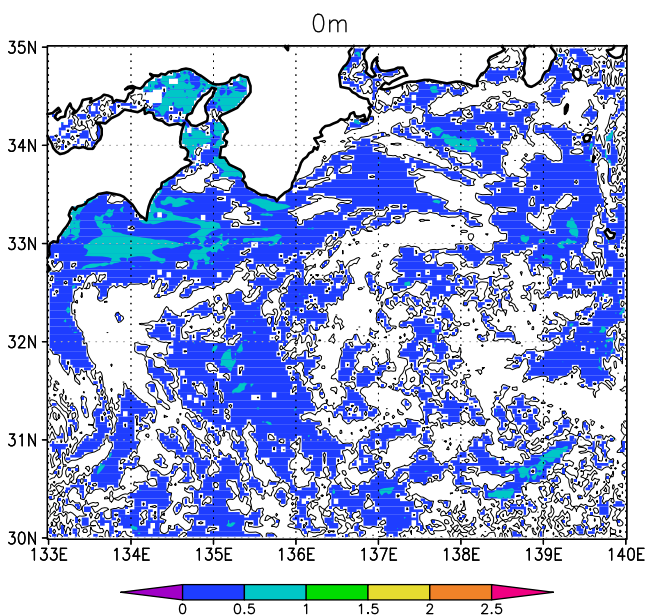
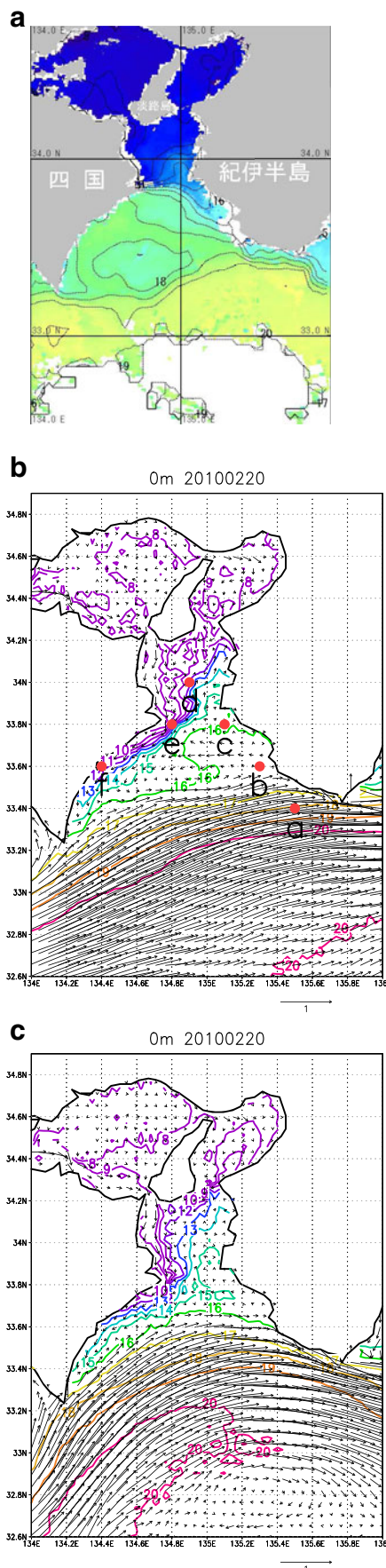


**Fig. 11** Reduction rate (7) of the analysis ensemble spread for sea surface temperature averaged for the period from 8 to 28 February 2010

shown in the observation (Fig. 12a). Comparison between the ENKF (Fig. 12b) and FRF (Fig. 12c) forecasts indicates that EnKF modified the Kuroshio path and removed warm bias inside of the Kii Channel. The assimilation of the observation data around the Kii Channel Front (Fig. 8) effectively reproduced the steep front structure. However, ENKF (Fig. 12b) seemed to fail the temperature gradient along the west coast of the Kii Peninsula and have cold bias along the east cost of the Shikoku Island as compared to the composite observation (Fig. 12a).

We calculated the ensemble heat budgets at points around the Kii Channel (see points in plotted in Fig. 12b) of the forecasts starting from the ENKF analyses on 0.00, 18 February 2010 (Fig. 13). Around of the Kuroshio northern edge (Fig. 13a), the ensemble mean forecast temperatures were around 18°C and their tendencies were basically determined by the advection (left panel of Fig. 13a). The ensemble mean advection terms show positive (negative) east–west (vertical) heat advection terms (right panel of Fig. 13a), confirming that the Kuroshio frontal variations dominantly governed the heat budget there. At a point along the west coast of the Kii Peninsula (Fig. 13b), negative vertical diffusion terms including the surface heat flux were slightly dominant over the advection terms and temperature values gradually decreased (left panel of Fig. 13b). The

**Fig. 12** **a** A composite map of satellite sea surface temperature on 20 February 2010 provided by the fishery research institute of Tokushima Prefecture. **b** Ensemble mean sea surface temperature (contours) and flows (vectors) of the ensemble forecasts on 20 February 2010 starting from the EnKF analyses on 18 February 2010. **c** Same as Fig. 12 b except for FRF



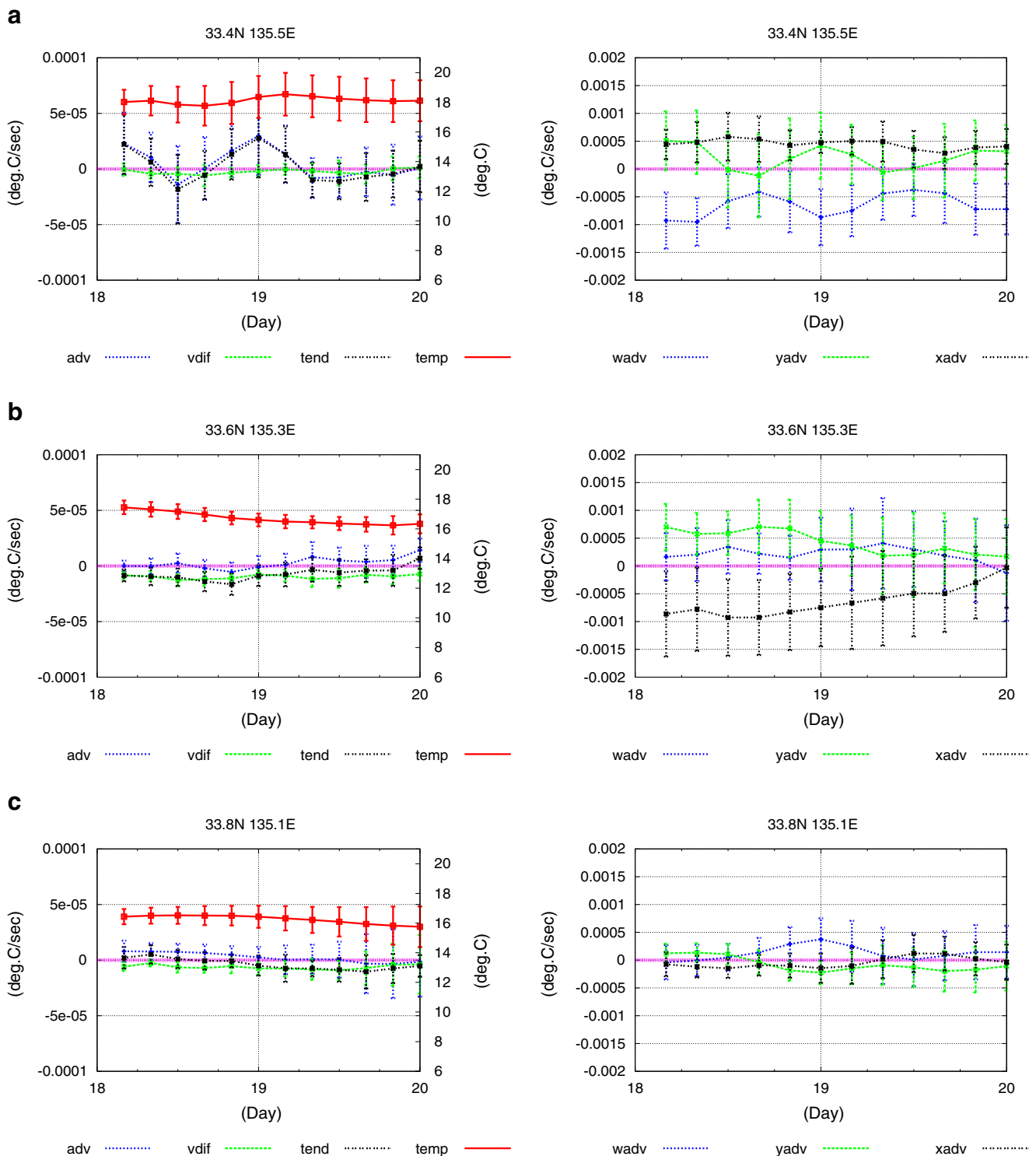


**Fig. 13** Left time sequences of 4-hourly ensemble mean sea surface temperature (thick lines), advection terms of temperature transport equation (dotted lines), vertical diffusion terms including surface heat flux effect (dashed lines), tendency terms (double-dotted lines) from the ensemble forecasts initialized by the ENKF analyses on 0:00, 18 February 2010 at **a** 33.4° N, 135.5° E, **b** 33.6° N, 135.3° E, **c** 33.8° N,

135.1° E, **d** 34.0° N, 134.9° E, **e** 33.8° N 134.8° E, and **f** 33.6° N 134.4° E. Horizontal diffusion terms were not plotted here because their magnitudes were small. Error bars denote the ensemble spread of the variables. Right as in left panels except for vertical advection terms (short dashed lines), north–south advection terms (long dashed lines), and east–west advection terms (double-dotted lines)

advection terms (right panel of Fig. 13b) indicates positive (negative) north–south (east–west) advection terms that

were consistent with the Kuroshio water intrusion along the west coast of the Kii Peninsula. A point inside of the

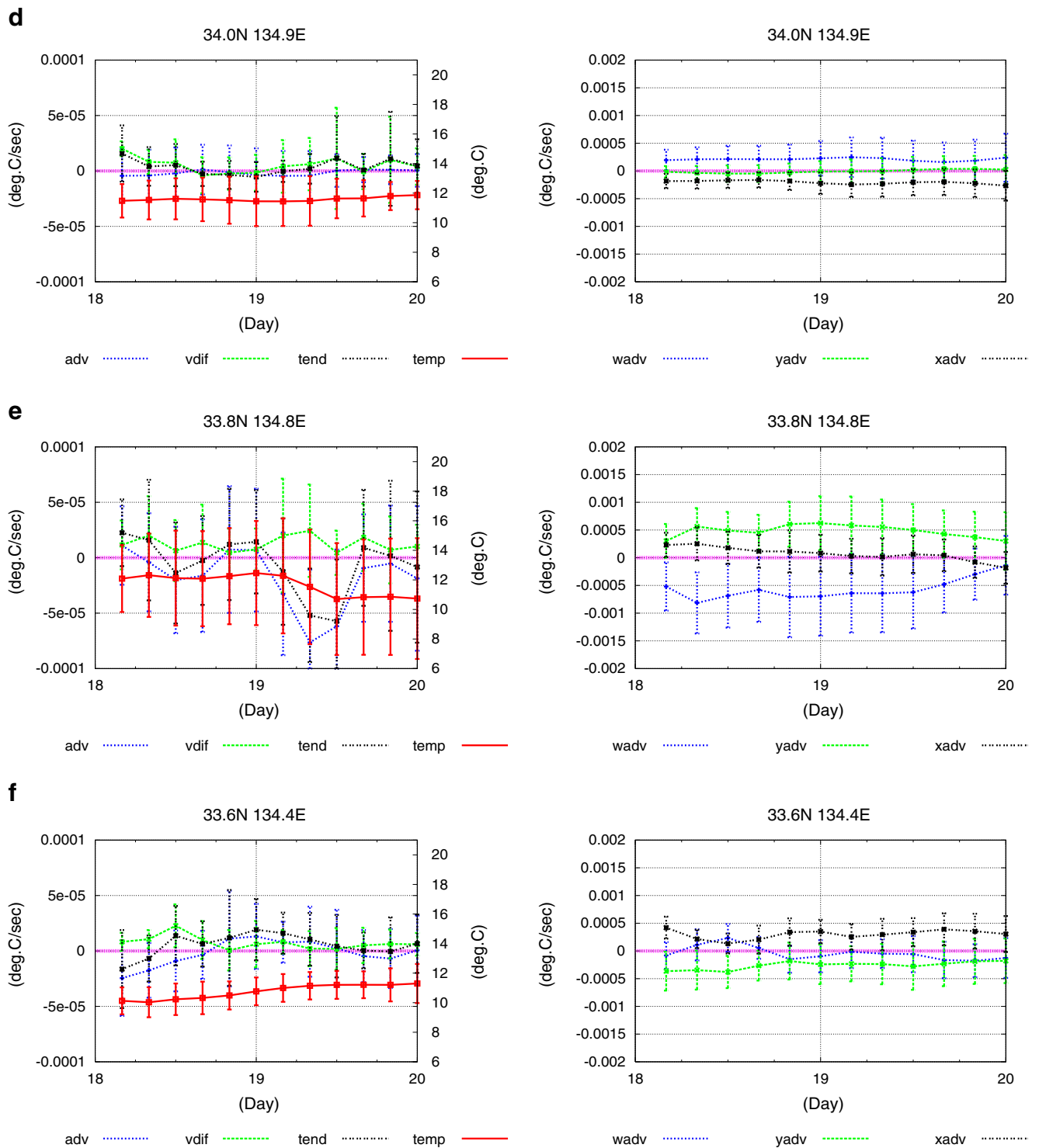


Fig. 13 (continued)

channel (Fig. 13c) shows the similar features but the weaker advection compared to the southern point (Fig. 13b). At a point around the front (Fig. 13d), the tendency was basically determined by the vertical diffusion including the surface heat flux effect (left panel of Fig. 13d) and positive

(negative) vertical (east–west) advection terms balanced to each other (right panel of Fig. 13d). Around the steep front (Fig. 13e), large amplitude of the spread indicates that the forecast values were significantly scattered and temporally variable due to the advection (left panel of Fig. 13e).

Positive (negative) horizontal (vertical) advection terms (right panel of Fig. 13e) suggest the warm water tended into the colder side of the front. At a point along the east coast of the Shikoku Island (Fig. 13f), positive vertical diffusion including the surface heat flux effect tended to increase temperature values (left panel of Fig. 13f) and negative (positive) north–south (east–west) advection terms almost balanced to each other (right panel of Fig. 13f), suggesting that the cold (warm) water was transported from the northern (eastern) region by the current.

In summary, ENKF reproduced the two types of front variations: the Kuroshio northern edge (Fig. 13a) and the Kii Channel Front (Figs. 13d, e), the Kuroshio water intrusion along the west coast of the Kii Peninsula (Figs. 13b, c), and its relevant circulation along the east coast of the Shikoku Island (Fig. 13f). The ensemble heat budget of FRF indicates that it failed to reproduce the anti-clockwise circulation due the Kuroshio intrusion and steep front variations (not shown). Slight difference between the composite observation (Fig. 12a) and ENKF ensemble mean forecast (Fig. 12b) near the coasts of the Kii Peninsula and Shikoku Island suggests more requirements of the observation data around there (see Fig. 8). The less predictability around the steep front was clearly indicated by the larger amplitude of the spread (Fig. 13e).

## 6 Summary and discussion

This study demonstrates the feasibility of the ensemble Kalman filter to the investigation of the real Kuroshio variations south of Japan in February 2010. We assimilated satellite sea surface height anomaly, satellite sea surface temperature, and in situ temperature and salinity profiles into an ocean general circulation model with horizontal resolution of  $1/36^\circ$  using EnKF. Twenty ensemble members of 2-day lead forecasts were updated by EnKF for the period from 8 to 28 February 2010. EnKF well reproduced the Kuroshio path positions. Also, EnKF well reproduced the observed water mass property in the Kuroshio region with RMSD of temperature and salinity smaller than  $1^\circ\text{C}$  and 0.1 psu, respectively.

The impacts of the assimilation of localized in situ observation data spread over the whole model region. The data impacts dynamically propagated from their origins to far owing to the effects of the temporally and spatially variable forecast error covariance represented by EnKF. In particular, EnKF effectively assimilated the in situ temperature and salinity data to represent the sharp structure of the Kii Channel Front and its variation affected by the warm water intrusion from the Kuroshio region. The ensemble heat budget analysis for the period from 18 to 20 February 2010 demonstrates

that EnKF generally reproduced the warm water intrusion into the channel in this period as observed. EnKF suggested that the variation around the steep front was comparatively unpredictable; more observations and inclusion of non-hydrostatic dynamics with higher horizontal resolution (Akitomo et al. 1990) were required for more exact representation of the variation of the steep front.

So far, the data assimilation methods used in operational ocean forecasting models for south of Japan have basically assumed time-constant and isotropic error covariance based on empirical knowledge of the oceanic conditions there (e.g., Miyazawa et al. 2008; 2009). This assumption is acceptable for typical mesoscale variations such as the Kuroshio path variations and mesoscale eddies with temporal and spatial scales of O (10 days) and O (100 km), respectively (Kuragano and Kamachi 2000). However, recent efforts of downscale modeling have allowed us to simulate the open and coastal seas interactions with highly variable temporal and anisotropic spatial scales due to coexistence of multi-scales phenomena (Isobe et al 2010). In particular, the interactions between the currents and coastal topography (Miyama and Miyazawa 2010) enhance the anisotropic features of horizontal scales of the phenomena. In such cases, the assumption is not valid. Our study demonstrates that EnKF is quite effective for detection of the open and coastal seas interactions because of its ‘seamless’ representation of the forecast error covariance from meso- to sub-mesoscales. Some diagnostic methods for the evaluation of the error covariance based on the model dynamics have been already discussed in the literature (e.g., Jameson et al. 2002). Skill comparison of EnKF with combinations of the operational data assimilation and the diagnostic methods will be useful for improvements of the existing operational ocean forecast systems in terms of representation of the open and coastal seas interactions.

Localization scales of the observation data are important parameters of LEKF (Miyoshi et al. 2010). For example, we used horizontal radius of  $1/3^\circ$  (Table 1) as the horizontal localization scale. This value was determined based on the results of the sensitivity experiments with pseudo-observation data sampled from the simulation (‘identical twin experiments’). Figure 10 depicts that the large values of covariance were found far away from the target point with more than  $1/3^\circ$  distance. But the representation of the error covariance was highly temporally and spatially variable. The corresponding error covariance distribution on 20 February 2010 showed quite smaller values around the target point (not shown), suggesting weak correlations between the target and surrounding points at this time. The present parameter of  $1/3^\circ$  is considered as a representative one averaged over the whole simulation period, whole model region, and all variables.

**Acknowledgments** This work is part of the Japan Coastal Ocean Predictability Experiment (JCOPE) promoted by the Japan Agency for Marine-Earth Science and Technology (JAMSTEC). The code of the local ensemble transformation Kalman filter (LETKF) was obtained from <http://code.google.com/p/miyoshi/>, which is maintained by Dr. Takamasa Miyoshi. Sea surface height anomaly data of Jasons-1 and Jasons-2 and sea surface temperature of NOAA MCSST were downloaded from the US-GODAE website: <http://www.usgodae.org/>. AMSR-E data were produced by remote sensing systems and sponsored by the NASA Earth Science MEaSUREs DISCOVER Project and the AMSR-E Science Team. Data are available at <http://www.remss.com/>. In situ temperature and salinity profiles were obtained from the Global Temperature-Salinity Profile Program (GTSP) website: <http://www.nodc.noaa.gov/GTSP/>. Comments from two anonymous reviewers were useful for improvements of the earlier version of the manuscript.

## References

- Akitomo K, Imasato N, Awaji T (1990) A numerical study of a shallow sea front generated by buoyancy flux: generation mechanism. *J Phys Oceanogr* 20:172–189
- Cohn SE (1997) An introduction to estimation theory. *J Meteor Soc Jpn* 75:257–288
- Conkright ME, Antonov JI, Baranova O, Boyer TP, Garcia HE, Gelfeld R, Johnson D, Locarnini RA, Murphy PP, O'Brien TD, Smolyar I, Stephens C (2002) World Ocean Database 2001, vol1: Introduction. In: Levitus S (ed) NOAA Atlas NESDIS 42. US Government Printing Office, Washington, p 167
- Evensen G (1994) Sequential data assimilation with a nonlinear quasi-geostrophic model using Monte-Carlo methods to forecast error statistics. *J Geophys Res* 99:10143–10162
- Evensen G (2003) The ensemble Kalman filter: theoretical formulation and practical implementation. *Ocean Dyn* 53:343–367
- Harashima A, Oonishi Y (1981) The Coriolis effect against frontogenesis in steady buoyancy-driven circulation. *J Oceanogr Soc Jpn* 37:49–59
- Hunt BR, Kostelich EJ, Szunyogh I (2007) Efficient data assimilation for spatiotemporal chaos: a local ensemble transform Kalman filter. *Physica D* 230:112–126
- Isobe A, Guo X, Takeoka H (2010) Hindcast and predictability of sporadic Kuroshio–water intrusion (kyucho in the Bungo Channel) into the shelf and coastal waters. *J Geophys Res* 115:C04023. doi:10.1029/2009JC005818
- Jameson L, Waseda T, Mitsudera H (2002) Scale utilization and optimization from wavelet analysis for data assimilation: SUGOiWADaI. *J Atmos Oceanic Tech* 19:747–758
- Kagimoto T, Miyazawa Y, Guo X, Kawajiri H (2008) High resolution Kuroshio forecast system: description and its applications. In: Hamilton K, Ohfuchi W (eds) High resolution numerical modeling of the atmosphere and ocean. Springer, New York, pp 209–239
- Kuragano T, Kamachi M (2000) Global statistical space-time scales of oceanic variability estimated from the TOPEX/POSEIDON altimetry data. *J Geophys Res* 105:955–974. doi:10.1029/1999JC900247
- Lorenz EN (1963) Deterministic nonperiodic flow. *J Atmos Sci* 20:130–141
- Miyama T, Miyazawa Y (2010) Sudden acceleration of Kuroshio jet off the Cape Shionomisaki in JCOPE2 ocean reanalysis data. Abstracts of 2010 Ocean Sciences Meeting, PO23
- Miyazawa Y, Yamane S, Guo X, Yamagata T (2005) Ensemble forecast of the Kuroshio meandering. *J Geophys Res* 110:C10026. doi:10.1029/2004JC002426
- Miyazawa Y, Kagimoto T, Guo X, Sakuma H (2008) The Kuroshio large meander formation in 2004 analyzed by an eddy-resolving ocean forecast system. *J Geophys Res* 113:C10015. doi:10.1029/2007JC004226
- Miyazawa Y, Zhang R, Guo X, Tamura H, Ambe D, Lee J-S, Okuno A, Yoshinari H, Setou T, Komatsu K (2009) Water mass variability in the western North Pacific detected in a 15-year eddy resolving ocean reanalysis. *J Oceanogr* 65:737–756
- Miyoshi T, Sato Y, Kadowaki T (2010) Ensemble Kalman Filter and 4D-Var intercomparison with the Japanese operational global analysis and prediction system. *Mon Wea Rev* 138:2846–2866
- Moteki Q, Yoneyama K, Shirooka R, Kubota H, Yasunaga K, Suzuki J, Seiki A, Sato N, Enomoto T, Miyoshi T, Yamane S. (2011) The influence of observations propagated by convectively coupled equatorial waves. *Quart J Royal Meteor Soc* 137:641.655. doi:10.1002/qj.779
- Toda T (1992) Double structure of the coastal front in the Kii Channel, Japan, during winter. *J Geophys Res* 97:11333–11342
- Vignudelli S, Cipollini P, Astraldi M, Gasparini GP, Manzella G (2000) Integrated use of altimeter and in situ data for understanding the water exchange between the Tyrrhenian and Ligurian Seas. *J Geophys Res* 105:19649–19663
- Wang D, Liu Y, Qi Y, Shi P (2001) Seasonal variability of thermal fronts in the northern South China Sea from satellite data. *Geophys Res Lett* 28:3963–3966
- Xie X, Iwata S, Nemoto M, Nagashima H (2006) A method for obtaining daily high-resolution sea surface temperature in the KUROSHIO regions. *Bull Japanese Soc Fish Oceanogr* 70:122–130 (in Japanese)
- Yanagi T, Sanuki T (1991) Variation in the thermohaline front at the mouth of Tokyo Bay. *J Oceanogr Soc Jpn* 47:105–110
- Yanagi T, Guo X, Saino T, Ishimaru T, Noriki S (1997) Thermohaline front at the mouth of Ise Bay. *J Oceanogr* 53:403–409
- Yosioka H (1983) Sea surface temperature and its application to the investigation of oceanic condition in Kii-Channel. *J Marine Meteorol Society Japan* ('Umi to Sora') 58:37–51 (in Japanese)